PAPER

Intrinsic rotation driven by turbulent acceleration

IOP Publishing Plasma Physics and Controlled Fusion
Plasma Phys. Control. Fusion **61** (2019) 025003 (9pp) https://doi.org/10.1088/1361-6587/aaeb69

Intrinsic rotation driven by turbulent acceleration

M Barnes[1,2] **and F I Parra**[1,2]

[1] Rudolf Peierls Centre for Theoretical Physics, University of Oxford, Clarendon Laboratory, Parks Road, Oxford OX2 3PU, United Kingdom
[2] Culham Centre for Fusion Energy, Abingdon OX14 3EA, United Kingdom

E-mail: michael.barnes@physics.ox.ac.uk

Received 4 August 2018, revised 22 September 2018
Accepted for publication 25 October 2018
Published 22 November 2018

Abstract

Differential rotation is induced in tokamak plasmas when an underlying symmetry of the governing gyrokinetic-Maxwell system of equations is broken. One such symmetry-breaking mechanism is considered here: the turbulent acceleration of particles along the mean magnetic field. This effect, often referred to as the 'parallel nonlinearity', has been implemented in the δf gyrokinetic code `stella` and used to study the dependence of turbulent momentum transport on the plasma size and on the strength of the turbulence drive. For JET-like parameters with a wide range of driving temperature gradients, the momentum transport induced by the inclusion of turbulent acceleration is similar to or smaller than the ratio of the ion Larmor radius to the plasma minor radius. This low level of momentum transport is explained by demonstrating an additional symmetry that prohibits momentum transport when the turbulence is driven far above marginal stability.

Keywords: gyrokinetics, intrinsic rotation, momentum transport

(Some figures may appear in colour only in the online journal)

1. Introduction

Observational evidence obtained from a wide range of tokamaks indicates that axisymmetric plasmas exhibit differential toroidal rotation even in the absence of an externally applied torque (see [1–11]). This 'intrinsic rotation' is determined by momentum redistribution within the plasma, which is typically dominated by turbulent transport. Understanding turbulent momentum transport is thus critical for predicting intrinsic rotation.

Calculation of the intrinsic turbulent momentum transport in tokamak plasmas is particularly challenging. This is the result of a symmetry of the gyrokinetic-Maxwell system of equations that statistically prohibits momentum transport to lowest order in the gyrokinetic expansion parameter $\rho_* \doteq \rho_i/a$, with ρ_i the ion Larmor radius and a the plasma minor radius [12–15]. The symmetry is broken by various physics effects that are formally small in ρ_* and thus neglected in standard δf gyrokinetic simulations. A comprehensive theory including all of these symmetry-breaking mechanisms is given in [15–19]. There have also been a number of studies dedicated to individual mechanisms, including the effect of diamagnetic flows [20–24], up–down asymmetry of flux surfaces [25–31], slow poloidal variation of fluctuations [32], and 'global' effects [33–36], which include radial profile variation mingled with the other effects mentioned. Here we consider the effect of turbulent particle acceleration along the mean magnetic field, which has not been studied before in the context of intrinsic momentum transport[3].

With the exception of up–down asymmetry of flux surfaces, all of the symmetry-breaking mechanisms drive momentum transport proportional to ρ_*. In the absence of additional scaling factors to increase the size of the momentum transport, the intrinsic rotation itself is thus a factor of ρ_* smaller than the sonic rotation—making it dynamically unimportant. However, as shown in [15], the intrinsic momentum transport arising from the various symmetry-breaking mechanisms is theoretically expected to scale with additional factors such as the driving gradients and the ratio

[3] The effect of turbulent acceleration on turbulent fluctuations has previously been considered [37, 38] and ultimately was shown to be small in ρ_* [39], as expected from the gyrokinetic orderings introduced in section 2.

of the total to poloidal magnetic field strength, B/B_p. In particular, neoclassical flow effects and finite-orbit-width effects drive turbulent momentum transport of size $\Pi_{\rm int}/\Pi_{\rm gB} \sim (k_\perp \rho_i)(B/B_p)\rho_*$, with $\Pi_{\rm int}$ the radial component of the toroidal angular momentum flux due to symmetry-breaking, $k_\perp$ the characteristic wavenumber of the turbulence in the plane perpendicular to the mean magnetic field, $\Pi_{\rm gB} \doteq \rho_*^2 pR$, p the total plasma pressure, and R the plasma major radius. The remaining effects—slow poloidal variation of turbulence, radial profile variation, and turbulent acceleration—drive turbulent momentum transport of size $\Pi_{\rm int}/\Pi_{\rm gB} \sim (k_\perp \rho_i)^{-2}\rho_*$. When turbulent eddies are sufficiently large, i.e. $k_\perp \rho_i \sim B_p/B$, all symmetry-breaking mechanisms are the same size. In principle, this may make it possible to drive intrinsic rotation at levels that, while still sub-sonic, can stabilize MHD modes and potentially suppress turbulence.

In this paper, we use the local, δf gyrokinetic code `stella` [40] to simulate electrostatic plasma turbulence, including the effect of turbulent particle acceleration (often referred to as the parallel nonlinearity). Both ρ_* and the driving temperature gradients are varied in order to determine the scalings of the intrinsic momentum flux and to thus determine the significance of turbulent acceleration in driving intrinsic rotation. Our results are compared with the theoretical scalings provided in [15], and discrepancies are explained via an additional approximate symmetry satisfied by the fluctuations far above marginal stability.

The paper is organised as follows. In section 2 we introduce the gyrokinetic-Poisson system of equations and the associated symmetry that prohibits momentum transport. We then discuss turbulent acceleration and show how it breaks the symmetry of the equations in section 3. We provide simple scalings for the intrinsic momentum flux due to this symmetry-breaking in section 4 before arguing for the existence of an additional, approximate symmetry satisfied by the system in section 5. Numerical results are presented in section 6, and a summary with discussion of implications is given in section 7.

2. Symmetry of the gyrokinetic-Poisson system

Low-frequency fluctuations in tokamak plasmas are described by the gyrokinetic-Maxwell system of equations [41–46]. They are obtained by averaging over particle gyration about the mean magnetic field, with the assumption that fluctuations evolve on a much longer time scale than the gyration period. If one further assumes a space-time scale separation between the fluctuations and the mean plasma profiles, then one obtains the local, δf gyrokinetic model. Explicitly, we restrict our attention to electrostatic fluctuations and impose the ordering

$$\frac{\delta f_s}{f_s} \sim \frac{\omega}{\Omega_s} \sim \frac{\rho_s}{L} \sim \frac{k_\parallel}{k_\perp} \sim k_\parallel \rho_s \sim \frac{e\hat{\varphi}}{T_s} \sim \epsilon \ll 1, \tag{1}$$

where ϵ is the fundamental gyrokinetic expansion parameter, $f_s = F_s + \delta f_s$ is the particle distribution function for species s, F_s and δf_s are its mean and fluctuating components, $\hat{\varphi}$ is the electrostatic potential, ω is a characteristic fluctuation frequency, $\Omega_s = Z_s eB/m_s c$ is the Larmor frequency, Z_s is particle charge number, m_s is particle mass, c is the speed of light, e is the proton charge, B is the magnetic field strength, $\rho_s = v_{{\rm th},s}/\Omega_s$ is the thermal Larmor radius, $v_{{\rm th},s} = \sqrt{2T_s/m_s}$, T_s is temperature, L is a characteristic length associated with mean plasma profiles, and $k_\parallel$ and $k_\perp$ are characteristic fluctuation wavenumbers along and across the mean magnetic field.

Gyro-averaging the Fokker–Planck equation, applying the gyrokinetic ordering (1), and expanding $f = f_0 + f_1 + f_2 + ...$, with $f_\alpha = {\rm O}(\epsilon^\alpha) f$, yields a gyrokinetic equation describing the evolution of $\hat{g}$, the distribution of particle guiding centres. We choose to work in $(\mathbf{R}, u, \mu, \vartheta)$ coordinates, with $\mathbf{R}$ the particle guiding centre position, $\mu = mv_\perp^2/2B$ the lowest order particle magnetic moment, u the particle velocity along the magnetic field, $v_\perp$ the particle speed across the magnetic field, respectively, and ϑ the particle gyrophase. In these coordinates the gyrokinetic equation valid to lowest order in ϵ is

$$\begin{aligned}
&\frac{\partial \hat{g}_{1s}}{\partial t} + u\hat{\mathbf{b}} \cdot \left(\nabla \hat{g}_{1s} + \frac{Z_s e}{T_s} F_{0s} \nabla \langle \hat{\varphi}_1 \rangle_{\mathbf{R}} \right) \\
&\quad + \mathbf{v}_{Ms} \cdot \left(\nabla_\perp \hat{g}_{1s} + \frac{Z_s e}{T_s} F_{0s} \nabla_\perp \langle \hat{\varphi}_1 \rangle_{\mathbf{R}} \right) \\
&\quad + \dot{u}_{0s} \frac{\partial \hat{g}_{1s}}{\partial u} + \frac{c}{B} \{ \langle \hat{\varphi}_1 \rangle_{\mathbf{R}}, \hat{g}_{1s} \} \\
&\quad + \langle \mathbf{v}_{E1} \rangle_{\mathbf{R}} \cdot \nabla|_E F_{0s} = \hat{C}[\hat{g}_{1s}],
\end{aligned} \tag{2}$$

where $\langle . \rangle_{\mathbf{R}}$ denotes a gyro-average at fixed guiding centre position $\mathbf{R}$, $\hat{\varphi}_1$ is the electrostatic potential generated by $\hat{g}_1$, t is time, $\hat{\mathbf{b}}$ is the unit vector along the mean magnetic field, F_{0s} is taken to be a Maxwellian distribution in particle velocity, $\dot{u}_{0s} = -(\mu/m_s)\hat{\mathbf{b}} \cdot \nabla B$ is the lowest order contribution to the parallel acceleration, $\nabla|_E$ is a gradient taken at fixed particle kinetic energy $E = mu^2/2 + \mu B$, $\mathbf{v}_{E1} = (c/B)\hat{\mathbf{b}} \times \nabla_\perp \hat{\varphi}_1$ is the $E \times B$ drift velocity, $\{.,.\}$ is a Poisson bracket, $\mathbf{v}_{Ms} = (\hat{\mathbf{b}}/\Omega_s) \times (\mu \nabla B + u^2 \boldsymbol{\kappa})$, $\boldsymbol{\kappa} = \hat{\mathbf{b}} \cdot \nabla \hat{\mathbf{b}}$, and the operator $\hat{C}$ accounts for the effect of collisions on $\hat{g}_1$. The system is closed by coupling to Poisson's equation, which reduces to quasineutrality when the Debye length is much smaller than the electron Larmor radius:

$$\sum_s Z_s e \int {\rm d}^3 v \left(\hat{g}_{1s} + \frac{Z_s e}{T_s} (\langle \hat{\varphi}_1 \rangle_{\mathbf{R}} - \hat{\varphi}_1) F_{0s} \right) = 0. \tag{3}$$

It will be convenient for much of the paper to work in Fourier space, so we define the Fourier components of $\hat{g}$ via $g_{\mathbf{k}} \doteq \mathcal{F}_{\mathbf{k}}[\hat{g}]$, with $\mathcal{F}_{\mathbf{k}}$ denoting the two-dimensional, discrete Fourier transform in the plane perpendicular to $\hat{\mathbf{b}}$ and $\mathbf{k}$ denoting the wave vector in this plane. We use the coordinate system (α, ψ, θ) to represent physical space, with ψ a flux surface label, α a field line label, and θ a poloidal angle measuring distance along a given magnetic field line.

Applying $\mathcal{F}_{\mathbf{k}}$ to (2) and (3) gives

$$\frac{\partial g_{1s,\mathbf{k}}}{\partial t} + u\hat{\mathbf{b}}\cdot\nabla\theta\left(\frac{\partial g_{1s,\mathbf{k}}}{\partial\theta} + \frac{Z_s e}{T_s}\frac{\partial J_0(a_{k,s})\varphi_{1,\mathbf{k}}}{\partial\theta}F_{0s}\right) + \mathrm{i}\mathbf{v}_{Ms}\cdot\mathbf{k}\left(g_{1s,\mathbf{k}} + \frac{Z_s e}{T_s}F_{0s}J_0(a_{k,s})\varphi_{1,\mathbf{k}}\right) + \dot{u}_{0s}\frac{\partial g_{1s,\mathbf{k}}}{\partial u} + \frac{c}{B}\mathcal{F}_{\mathbf{k}}[\{\langle\hat{\varphi}_1\rangle_{\mathbf{R}}, \hat{g}_{1s}\}] + \mathrm{i}k_\alpha c J_0(a_{k,s})\varphi_{1,\mathbf{k}}\frac{\partial F_{0s}}{\partial\psi}\Big|_E = C_{\mathbf{k}}[g_{1s,\mathbf{k}}], \tag{4}$$

and

$$\sum_s Z_s e\left(\int \mathrm{d}^3 v J_0(a_{k,s})g_{1s\mathbf{k}} + \frac{Z_s e n_s}{T_s}(\Gamma_0(b_{k,s}) - 1)\varphi_{1,\mathbf{k}}\right) = 0, \tag{5}$$

where n_s is the plasma density, J_0 is a Bessel function of the first kind, $a_{k,s} = kv_\perp/\Omega_s$, $\Gamma_0(b) = \exp(-b)I_0(b)$, I_0 is a modified Bessel function of the first kind, $b_{k,s} = k^2\rho_s^2/2$, and $C_{\mathbf{k}}[g_{1s,\mathbf{k}}] \doteq \mathcal{F}_{\mathbf{k}}[\hat{C}[\hat{g}_{1s}]]$.

If the confining magnetic geometry is up–down symmetric, the gyrokinetic-Poisson system (4) and (5) possesses a symmetry that inhibits momentum transport: If $g_{1s}(k_\psi, k_\alpha, \theta, u, \mu, t)$ is a solution with associated potential $\varphi_1(k_\psi, k_\alpha, \theta, t)$, then $g_{1s}^{\leftrightarrow}(k_\psi, k_\alpha, \theta, u, \mu, t) = -g_{1s}(-k_\psi, k_\alpha, -\theta, -u, \mu, t)$ is also a solution with associated potential $\varphi_1^{\leftrightarrow}(k_\psi, k_\alpha, \theta, t) = -\varphi_1(-k_\psi, k_\alpha, -\theta, t)$ [12–15]. For turbulence in a statistical steady state that is independent of initial conditions, g_{1s} and $g_{1s}^{\leftrightarrow}$ occur with equal frequency. Upon statistical average, this leads to a vanishing lowest-order, radial transport of toroidal angular momentum $\Pi_1 = \langle|\nabla\psi|\rangle_\psi^{-1}\int \mathrm{d}^3 v\langle(mR^2\delta f\mathbf{v}\cdot\nabla\zeta)(\mathbf{v}_E\cdot\nabla\psi)\rangle_\psi$, where ζ is toroidal angle, $\langle A\rangle_\psi \doteq \left(\int \mathrm{d}\zeta\mathrm{d}\theta\mathcal{J}\right)^{-1}\int \mathrm{d}\zeta\mathrm{d}\theta\mathcal{J}A$ denotes an average over the flux surface, and $\mathcal{J} = \mathbf{B}\cdot\nabla\theta$ is the Jacobian of the transform to (ζ, ψ, θ) coordinates. The statistical average could be a time average over many nonlinear decorrelation times in a statistical steady state or an ensemble average over many turbulence realisations. We use the former definition in the simulation results that follow. The fact that Π_1 vanishes can be deduced by examining the contribution to Π_1 from wavevector $\mathbf{k}$, given by

$$\Pi_{1,\mathbf{k}} = -\frac{1}{\langle|\nabla\psi|\rangle_\psi}\sum_s\left\langle\frac{m_s c}{B}k_\alpha\varphi_{1,\mathbf{k}}^*\int \mathrm{d}^3 v g_{1s,\mathbf{k}} \times\left(\mathrm{i}uI(\psi)J_0(a_{k,s}) + \mathbf{k}\cdot\nabla\psi\frac{v_\perp^2}{\Omega_s}\frac{J_1(a_{k,s})}{a_{k,s}}\right)\right\rangle_\psi - \frac{1}{\langle|\nabla\psi|\rangle_\psi}\sum_s\left\langle\frac{m_s n_s c^2}{B^2}k_\alpha\mathbf{k}\cdot\nabla\psi\,|\varphi_{1,\mathbf{k}}|^2 \times(\Gamma_0(b_{\mathbf{k},s}) - \Gamma_1(b_{\mathbf{k},s}))\right\rangle_\psi, \tag{6}$$

with $I(\psi) = RB_\zeta$, R the plasma major radius, B_ζ the toroidal component of the magnetic field, $\Gamma_1(b) = \exp(-b)I_1(b)$, and $*$ denoting complex conjugation. Applying the symmetry discussed above, we see that the lowest order contribution to the radial flux of toroidal angular momentum, $\Pi_1 = \sum_{\mathbf{k}}\overline{\Pi_{1,\mathbf{k}}}$, is zero, with the overline denoting a statistical average.

3. Symmetry-breaking induced by turbulent acceleration

The symmetry of the lowest order gyrokinetic equation (4) is broken when one takes into account various physics effects that are formally small in the gyrokinetic expansion parameter ϵ [15, 16]. Here we focus on one such symmetry-breaking mechanism, the turbulent parallel acceleration of particles. Retaining higher order terms, the force parallel to the mean magnetic field is given by

$$m_s\dot{u}_s = -\left(\hat{\mathbf{b}} + \frac{u}{\Omega_s}\hat{\mathbf{b}}\times\boldsymbol{\kappa}\right)\cdot(\mu\nabla B + Z_s e\nabla\hat{\varphi}) + \mathcal{O}\left(\rho_{*s}^2\frac{T_s}{a}\right), \tag{7}$$

with a the minor radius of the plasma volume and $\rho_{*s} = \rho_s/a$. Defining $\dot{u}_{1s} = \dot{u}_s - \dot{u}_{0s} + \mathcal{O}(\rho_{*s}^2 v_{\mathrm{th},s}^2/a)$, we have

$$m_s\dot{u}_{1s} = -Z_s e\hat{\mathbf{b}}\cdot\nabla\hat{\varphi}_1 - \frac{u}{\Omega_s}\hat{\mathbf{b}}\times\boldsymbol{\kappa}\cdot(\mu\nabla B + Z_s e\nabla\hat{\varphi}_1). \tag{8}$$

We see that, in contrast to the lowest order parallel acceleration $\dot{u}_0$, the acceleration $\dot{u}_1$ is turbulent in nature; i.e. it depends on the fluctuating electrostatic potential $\hat{\varphi}_1$. The second term in (8) is the only one independent of turbulence amplitude, and it can be manipulated into the form $(\mu u/\Omega_s)\hat{\mathbf{b}}\times\boldsymbol{\kappa}\cdot\nabla B = \beta'(\mu u/\Omega_s)I\hat{\mathbf{b}}\cdot\nabla B$, with $\beta' \doteq (4\pi/B^2)\partial\, p_{\mathrm{tot}}/\partial\psi$ and p_{tot} the total plasma pressure. As the plasma pressure in tokamaks is small compared to the magnetic pressure, $|\beta'|$ is typically small. The parallel acceleration given by (8) is then dominated by the turbulent contributions.

The breaking of symmetry induced by inclusion of $\dot{u}_1$ can be seen by comparing how $\dot{u}_0$ and $\dot{u}_1$ behave under the transformation $(\theta\to-\theta, u\to-u, k_\psi\to-k_\psi)$. We see that $\dot{u}_0(\theta, u, k_\psi) = -\dot{u}_0(-\theta, -u, -k_\psi)$, while $\dot{u}_1(\theta, u, k_\psi) = \dot{u}_1(-\theta, -u, -k_\psi)$. This difference in parity Mars the symmetry described in section 2 and leads to finite steady-state momentum transport. Replacing $g_{1s,\mathbf{k}}$ with $g_{s,\mathbf{k}}$ and $\dot{u}_{0s}$ with $\dot{u}_s$ in (4) and (5), and defining $g_{2s,\mathbf{k}} \doteq g_{s,\mathbf{k}} - g_{1s,\mathbf{k}}$, the gyrokinetic-Poisson system becomes

$$\frac{\partial g_{2s,\mathbf{k}}}{\partial t} + u\hat{\mathbf{b}}\cdot\nabla\theta\left(\frac{\partial g_{2s,\mathbf{k}}}{\partial\theta} + \frac{Z_s e}{T_s}\frac{\partial J_0(a_{k,s})\varphi_{2,\mathbf{k}}}{\partial\theta}F_{0s}\right) + \mathrm{i}\mathbf{v}_{Ms}\cdot\mathbf{k}\left(g_{2s,\mathbf{k}} + \frac{Z_s e}{T_s}F_{0s}J_0(a_{k,s})\varphi_{2,\mathbf{k}}\right) + \dot{u}_{0s}\frac{\partial g_{2s,\mathbf{k}}}{\partial u} + \mathcal{F}_{\mathbf{k}}\left[\dot{u}_{1s}\frac{\partial\hat{g}_s}{\partial u} + \frac{c}{B}(\{\langle\hat{\varphi}\rangle_{\mathbf{R}}, \hat{g}_s\} - \{\langle\hat{\varphi}_1\rangle_{\mathbf{R}}, \hat{g}_{1s}\})\right] + \mathrm{i}k_\alpha c J_0(a_{k,s})\varphi_{2,\mathbf{k}}\frac{\partial F_{0s}}{\partial\psi}\Big|_E = C_{\mathbf{k}}[g_{2s,\mathbf{k}}] \tag{9}$$

and

$$\sum_s Z_s e\left(\int \mathrm{d}^3 v J_0(a_{k,s}) g_{2s\mathbf{k}} + \frac{Z_s e n_s}{T_s}(\Gamma_0(b_{k,s}) - 1)\varphi_{2,\mathbf{k}}\right) = 0. \tag{10}$$

For $g_{2s,\mathbf{k}} \ll g_{1s,\mathbf{k}}$, the product of $g_{2s,\mathbf{k}}$ and $\varphi_{2,\mathbf{k}}$ can be neglected when calculating the radial flux of toroidal angular momentum. The resulting expression for the lowest order (non-vanishing) momentum flux is $\Pi_2 = \sum_{\mathbf{k}} \Pi_{2,\mathbf{k}}$, with

$$\begin{aligned}\Pi_{2,\mathbf{k}} = &-\frac{1}{\langle|\nabla\psi|\rangle_\psi}\sum_s \left\langle \frac{m_s c}{B} k_\alpha \varphi^*_{2,\mathbf{k}} \int \mathrm{d}^3 v g_{1s,\mathbf{k}} \right. \\ &\times \left.\left(\mathrm{i}uI(\psi) J_0(a_{k,s}) + \mathbf{k}\cdot\nabla\psi \frac{v_\perp^2}{\Omega_s}\frac{J_1(a_{k,s})}{a_{k,s}}\right)\right\rangle_\psi \\ &- \frac{1}{\langle|\nabla\psi|\rangle_\psi}\sum_s \left\langle \frac{m_s c}{B} k_\alpha \varphi^*_{1,\mathbf{k}} \int \mathrm{d}^3 v g_{2s,\mathbf{k}} \right. \\ &\times \left.\left(\mathrm{i}uI(\psi) J_0(a_{k,s}) + \mathbf{k}\cdot\nabla\psi \frac{v_\perp^2}{\Omega_s}\frac{J_1(a_{k,s})}{a_{k,s}}\right)\right\rangle_\psi \\ &- \frac{2}{\langle|\nabla\psi|\rangle_\psi}\sum_s \left\langle \frac{m_s n_s c^2}{B^2} k_\alpha \mathbf{k}\cdot\nabla\psi \mathrm{Re}[\varphi^*_{1,\mathbf{k}}\varphi_{2,\mathbf{k}}] \right. \\ &\times \left.(\Gamma_0(b_{\mathbf{k},s}) - \Gamma_1(b_{\mathbf{k},s}))\right\rangle_\psi,\end{aligned} \tag{11}$$

where Re[.] denotes the real part.

4. Momentum flux scalings

We are interested in determining how the amplitude of the momentum flux scales with quantities such as device size, eddy size, and driving gradients. The expected amplitude of the momentum flux given by (11) depends on the fluctuation amplitudes and wavenumbers, as well as the phases between different fluctuations. To obtain the aforementioned scalings for the momentum flux, we must thus first deduce the scalings for the fluctuations. To do this we make a number of assumptions along the lines of [15, 47], where similar scalings for turbulent heat and momentum fluxes are obtained. In particular, we assume: that phase differences between $g_{\mathbf{k}}$ and $\varphi_{\mathbf{k}}$ lead to no more than order unity variations in the flux; that the fluctuations are isotropic in the plane perpendicular to the mean magnetic field so that $k_\alpha \alpha \sim k_\psi \psi \sim k_\perp \rho_i$; that at the outer scale the nonlinear transfer rate $\tau_{\mathbf{k}}^{-1}$ is comparable to the energy injection rate, which we estimate to be of order $k_\perp \rho_i v_{\mathrm{th}}/L_T$, with L_T the ion temperature gradient scale length; and that the plasma is in a state of critical balance [48] so that the time scale associated with parallel propagation $(k_\parallel v_{\mathrm{th}})^{-1}$ is comparable to the nonlinear turnover time $\tau_{\mathbf{k}}$ at all spatial scales.

Assuming $e\varphi_{1,\mathbf{k}}/T \sim g_{1s,\mathbf{k}}/F_{0s}$ and $\tau_{\mathbf{k}}^{-1} \sim (\mathbf{v}_E\cdot\nabla)_{\mathbf{k}} \sim (k_\perp\rho_i)^2 (v_{\mathrm{th}}/\rho_i)(e\varphi_{1,\mathbf{k}}/T)$, we obtain

$$k_\parallel v_{\mathrm{th}} \sim (k_y\rho_i)^2 \frac{v_{\mathrm{th}}}{\rho_i}\frac{e\varphi_{1,\mathbf{k}}}{T} \sim k_\perp \rho_i \frac{v_{\mathrm{th}}}{L_T}, \tag{12}$$

where we have taken $a \sim L_n \sim L_T$, with L_n the density gradient scale length. Balancing the first and last terms gives $k_\parallel L_T \sim k_\perp \rho_i$, and balancing the last two terms gives $e\varphi_{1,\mathbf{k}}/T \sim (k_\perp L_T)^{-1}$. If $k_\parallel$ is set by the system size, then these scalings predict that the characteristic $k_\perp$ of the turbulence decreases and that the fluctuation amplitudes rapidly increase with increasing temperature gradient. The same trends are obtained if instead the minimum $k_\perp$ is set by linear stability thresholds, which would make the minimum $k_\perp$ decrease with increasing temperature gradient. Gyrokinetic simulations of plasma turbulence far from marginal stability have found results consistent with these predictions [47].

Now that we have a predicted scaling for $\varphi_{1,\mathbf{k}}$—and thus $g_{1s,\mathbf{k}}$—we proceed to obtain the scaling for $g_{2s,\mathbf{k}}$. We argued above that the time scale associated with the fluctuations is $k_\perp \rho_i (v_{\mathrm{th}}/L_T)$. Using this time scale and balancing $\partial g_{2s,\mathbf{k}}/\partial t$ with the source terms containing $g_{1s,\mathbf{k}}$ and $\varphi_{1,\mathbf{k}}$ in (9), we have

$$\begin{aligned} k_\perp \rho_i \frac{v_{\mathrm{th}}}{L_T} g_{2s,\mathbf{k}} &\sim \mathcal{F}_{\mathbf{k}}\left[\dot{u}_{1s}\frac{\partial \hat{g}_1}{\partial u}\right] \sim \frac{v_{\mathrm{th}}}{L_T}\frac{\rho_i}{L_T} g_{1s,\mathbf{k}} \\ &\sim \frac{v_{\mathrm{th}}}{L_T}\left(\frac{\rho_i}{L_T}\right)^2 \frac{1}{k_\perp\rho_i} F_{0s}, \end{aligned} \tag{13}$$

from which we find $g_{2s,\mathbf{k}} \sim (k_\perp L_T)^{-2} F_{0s}$. Substituting the scalings for $g_{1s,\mathbf{k}}$, $g_{2s,\mathbf{k}}$, $\varphi_{1,\mathbf{k}}$, and $\varphi_{2,\mathbf{k}}$ into (11) gives

$$\frac{\Pi_{2,\mathbf{k}}}{Q_{1i,\mathbf{k}}}\frac{v_{\mathrm{th}}}{R} \sim \frac{\rho_i}{L_T}\frac{1}{k_\perp\rho_i}, \tag{14}$$

where the lowest-order contribution to the ion radial energy transport is $Q_{1i} = \sum_{\mathbf{k}} Q_{1i,\mathbf{k}}$, with

$$Q_{1s,\mathbf{k}} = -\frac{\mathrm{i}ck_\alpha}{\langle|\nabla\psi|\rangle_\psi}\left\langle \varphi^*_{1,\mathbf{k}} \int \mathrm{d}^3 v g_{1s,\mathbf{k}} J_0(a_{k,s})\left(\frac{m_s v^2}{2}\right)\right\rangle_\psi. \tag{15}$$

Our use of the ion energy flux to normalize $\Pi_{2,\mathbf{k}}$ in (14) is motivated by the fact that $\Pi_{1,\mathbf{k}} = 0$.

The scaling relation (14) implies that the intrinsic momentum flux arising from the turbulent parallel acceleration is always small in the gyrokinetic expansion parameter $\epsilon \sim \rho_i/L$ and is minimum near marginal stability where both $k_\perp$ and L_T are relatively large. However, as we discuss in section 5, an additional symmetry of the gyrokinetic-Poisson system may be approximately satisfied when both $k_\perp$ and L_T become sufficiently small. If so, the momentum transport induced by turbulent acceleration could be much smaller than the estimate given by (14).

5. Additional symmetry for reduced system

In a system with no magnetic shear and no magnetic drift in the radial direction, an additional symmetry of the gyrokinetic-Poisson system of equations exists. Namely, if $g_{1s}(k_\psi, k_\alpha, \theta, u, \mu, t)$ is a solution with associated potential $\varphi_1(k_\psi, k_\alpha, \theta, t)$, then $g_{1s}^{\leftrightarrow}(k_\psi, k_\alpha, \theta, u, \mu, t) = g_{1s}(k_\psi, k_\alpha, -\theta, -u, \mu, t)$ is also a solution with associated potential $\varphi_1^{\leftrightarrow}(k_\psi, k_\alpha, \theta, t) = \varphi_1(k_\psi, k_\alpha, -\theta, t)$ [15]. This differs from the symmetry of the full gyrokinetic-Poisson system in that there is no need to change the sign of the radial wavenumber k_ψ and of $\hat{g}_{1s}$ and $\hat{\varphi}_1$.

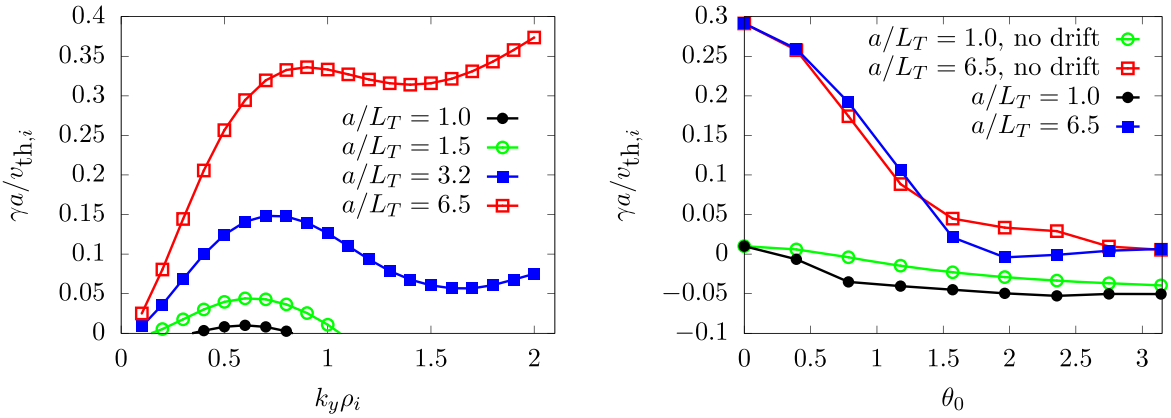

Figure 1. (Left): Normalized linear growth rate γ versus normalized bi-normal wavenumber $k_y\rho_i$ for $k_x = 0$ and different values of the equilibrium temperature gradient scale length L_T. (Right): Normalized linear growth rate γ versus ballooning angle $\theta_0 = k_x/k_y\hat{s}$ for $k_y\rho_i = 0.6$, with and without the radial component of the magnetic drift artificially set to zero.

While the parallel acceleration $\dot{u}_1$ breaks the full symmetry discussed in section 2, it does not break the symmetry of a system with neither magnetic shear nor a radial magnetic drift—as long as the second term in (8) can be neglected. As discussed in section 3, this is a good approximation when β' is small or the turbulence amplitude is large. Because of the additional symmetry of the reduced system, φ_1 does not change sign when $\theta \to -\theta$, and so $\dot{u}_1^{\leftrightarrow}(\theta, u) = -\dot{u}_1(-\theta, -u)$. This sign reversal under the transformation $(u, \theta) \to (-u, -\theta)$ is identical to the behavior of the lowest order acceleration $\dot{u}_0$ and thus does not break the symmetry of the reduced gyrokinetic-Poisson system. Consequently, the turbulent acceleration does not contribute to momentum transport.

Although the systems in which we are interested in general have both magnetic shear and a radial magnetic drift, it is still possible for this additional symmetry to be approximately satisfied. For systems far from marginal stability with $R/L_T \gg 1$, the radial magnetic drift often has only a small effect on linear growth rates and nonlinear physics; an illustrative example is provided in section 6 (see figure 1). A possible reason for this is the fact that the time scale associated with the radial magnetic drift is small compared to that of the background gradient drive (and thus the streaming and nonlinear turnover times via the critical balance argument of section 4) by a factor of R/L_T. When the radial magnetic drift is unimportant, the magnetic shear appears in the gyrokinetic-Poisson system only through the perpendicular wavenumber as an argument to the Bessel function. For turbulence peaked at long wavelengths—as we argue in section 4 is the case far from marginal stability—the Bessel function is approximately independent of $k_\perp$. In this limit the magnetic shear plays little role as well. It is thus possible that the additional symmetry described here is approximately satisfied as turbulence is driven beyond marginal stability. Consequently, it is expected that the momentum transport driven by parallel acceleration will be small for turbulence far from marginal stability.

6. Simulation equations and results

To test the predictions for the size of the momentum flux arising from the inclusion of turbulent acceleration, we have implemented the $\dot{u}_{1s}$ terms given by (8) in the local, δf gyrokinetic code `stella` [40]. For the sake of simulation efficiency, we do not separately evolve $g_{1s,\mathbf{k}}$ and $g_{2s,\mathbf{k}}$; instead, we simulate a single equation for $g_{s,\mathbf{k}} = g_{1s,\mathbf{k}} + g_{2s,\mathbf{k}}$, obtained by summing the two lowest order equations (4) and (9):

$$\frac{\partial g_{s,\mathbf{k}}}{\partial t} + u\hat{\mathbf{b}}\cdot\nabla\theta\left(\frac{\partial g_{s,\mathbf{k}}}{\partial\theta} + \frac{Z_s e}{T_s}\frac{\partial J_0(a_{k,s})\varphi_{\mathbf{k}}}{\partial\theta}F_{0s}\right) + \mathcal{F}_{\mathbf{k}}\left[\dot{u}_s\frac{\partial\hat{g}_s}{\partial u} + \frac{c}{B}\{\langle\hat{\varphi}\rangle_{\mathbf{R}}, \hat{g}_s\}\right] + \mathrm{i}\mathbf{v}_{Ms}\cdot\mathbf{k} \times\left(g_{s,\mathbf{k}} + \frac{Z_s e}{T_s}F_{0s}J_0(a_{k,s})\varphi_{\mathbf{k}}\right) + \mathrm{i}ck_\alpha J_0(a_{k,s})\varphi_{\mathbf{k}}\frac{\partial F_{0s}}{\partial\psi}\Bigg|_E = C_k[g_{s,\mathbf{k}}], \tag{16}$$

where the collision operator C_k used in `stella` is a gyrokinetic form [49] of the Dougherty collision operator [50], a Fokker–Planck operator that satisfies Boltzmann's H-Theorem and conserves particle number, momentum and energy. The associated quasineutrality constraint is identical to (5) with the substitution $g_{1s,\mathbf{k}} \to g_{s,\mathbf{k}}$. Note that we have implicitly included a number of terms at even higher order in (16) by including products of $\varphi_{2,\mathbf{k}}$ and $g_{2s,\mathbf{k}}$ in the nonlinearities. These should not affect our results, provided ϵ is sufficiently small.

For our simulations we use a Miller local specification of the magnetic geometry [51], in which the cylindrical coordinates R and Z are expressed as $R(r, \theta) = R_0(r) + r\cos(\theta + \sin\theta\arcsin\delta(r))$ and $Z(r, \theta) = \kappa(r)r\sin(\theta)$. Here κ and δ measure elongation and triangularity of the target flux surface, and r and R_0 are averages of the minimum and maximum values of the minor and major radii of the target flux surface at the height of the magnetic axis. The fixed parameter values used in our `stella` simulations, chosen to

Table 1. Equilibrium plasma parameters for `stella` simulations.

Parameter	Description	Value
$\tilde{r} = r/a$	Normalized minor radius	0.5
$\tilde{R} = R_0/a$	Normalized major radius	3.2
$\mathrm{d}R_0/\mathrm{d}r$	Local Shafranov shift	−0.2
q	Safety factor	1.7
$\hat{s} = d\ \ln q/d\ \ln r$	Magnetic shear	0.7
κ	Elongation	1.35
$\mathrm{d}\kappa/\mathrm{d}\tilde{r}$	Elongation derivative	0.1
δ	Triangularity	0.1
$\mathrm{d}\delta/\mathrm{d}\tilde{r}$	Triangularity derivative	0.2
$(4\pi p_{\mathrm{tot}}/B_r^2)(d\ \ln p_{\mathrm{tot}}/\mathrm{d}\tilde{r})$	Normalized β'	−0.035
$\nu_{ii}(a/v_{\mathrm{th},i})$	Ion–ion collision frequency	0.005
a/L_n	Inverse density gradient scale length	0.7
B_r	Reference magnetic field strength	RB_ζ/R_0

be similar to those of a typical JET shot at mid-radius, are given in table 1. In order to test our scaling predictions for the intrinsic momentum flux (14), we conducted scans in both ρ_* and a/L_T. These scans are intended to determine the intrinsic momentum flux as a function of plasma volume and distance from marginal stability, respectively.

All simulations discussed here treated electrons and a single deuterium ion species kinetically and used 48 grid points in u, 12 grid points in μ, and 32 grid points per 2π segment in θ. The results of linear simulations with $\rho_* = 0$ and a/L_T varying from 1 to 6.5 are given in figure 1. These simulations used an extended ballooning domain spanning $[-3\pi, 3\pi]$ in θ. We see from the growth rate spectrum that $a/L_T = 1$ is very near the linear critical gradient, with only a narrow range of weakly-unstable bi-normal mode numbers (k_y). In contrast, $a/L_T = 6.5$ is far above marginal stability, with relatively large growth rates across the entire spectrum and no finite cutoff at long wavelengths. In the former case, one anticipates that the largest turbulent eddies are determined by the minimum $k_\perp$ for which there is a non-zero growth rate; in the latter case, the largest turbulent eddies are constrained by the connection length along the magnetic field via the critical balance argument summarized in section 4. This range of a/L_T should thus give a good indication of how the intrinsic momentum flux varies with distance from marginality. The right-hand plot in figure 1, which shows the variation in growth rate as a function of the ballooning angle $\theta_0 \doteq k_x/(\hat{s}k_y)$, demonstrates the relative unimportance of the radial component of the magnetic drift for calculating the linear growth rate when the system has large R/L_T and is far from marginal stability.

Time-averaged fluxes from nonlinear simulations run with $\rho_* = 0.01$ and different a/L_T values are given in figure 2. After de-aliasing, the simulations included 128 Fourier modes in the radial wavenumber $k_x \doteq k_\psi r B_r/q$ and 22 Fourier modes in the bi-normal wavenumber $k_y \doteq k_\alpha B_r \mathrm{d}r/\mathrm{d}\psi$, with ψ the poloidal flux. The spacings in $k_y\rho_i$ and $k_x\rho_i$ were 0.05 and approximately 0.055 for all a/L_T values except $a/L_T = 6.5$, for which the spacings were approximately 0.033 and 0.037, respectively. From the left panel of figure 2, we see that the ratio of ion momentum flux Π to ion heat flux Q_i is approximately ρ_* near marginal stability and decreases as the system gets further from marginal stability.

The size of Π/Q_i near marginal stability is consistent with the scaling prediction given in (14), but its decrease with increasing a/L_T is not. This is not entirely surprising given the discussion in section 5 of an additional symmetry prohibiting momentum transport when the turbulence is concentrated at long wavelengths and when the radial magnetic drifts are unimportant. Indeed, this is borne out by considering the behavior of the gyro-Bohm-normalized ion heat flux. From the right panel of figure 2, we see that Q_i increases rapidly with distance from marginality, as expected. Artificially removing the radial component of the magnetic drift results in more than an order of magnitude change in the heat flux near marginal stability, but only a few tens of percent change far above marginal stability. When coupled with the fact that the turbulence peaks at wavelengths comparable to the poloidal Larmor radius far from marginality [47], this indicates that the additional symmetry discussed in section 5 should be approximately satisfied. From the left panel of figure 2, we see that the ratio Π/Q_i goes to zero (within error bars) when the radial magnetic drift is removed—consistent with the presence of the additional symmetry of section 5. This explains the small values of Π/Q_i for large a/L_T.

We consider the scaling of Π/Q_i with ρ_* at fixed $a/L_T = 3.2$ in figure 3. The data are consistent with a linear scaling in ρ_*, as expected for small ρ_* given the perturbative framework in which we are working.

7. Summary and discussion

The main results of the paper are encapsulated in figures 2 and 3. They indicate, for the parameters chosen here, that the radial transport of toroidal angular momentum driven by turbulent parallel acceleration is similar to or smaller than ρ_*, regardless of the strength of the turbulence drive. We argued in section 4 that this should be expected when turbulent eddies have a typical size of the ion gyroradius, as is the case near marginal stability. Further from marginal stability, as turbulent eddies grow larger, the same scaling arguments predict that the ratio of momentum flux to heat flux should increase. This discrepancy with simulation results is anticipated in section 5 by noting that an additional, approximate symmetry of the gyrokinetic-Poisson system is satisfied when β' is small, radial magnetic drifts are unimportant and turbulence is concentrated at long wavelengths. These conditions are often satisfied far above marginal stability, as borne out by the data presented in section 6.

To the extent that our results are applicable to a broader range of plasma parameters, our study implies that turbulent acceleration is unlikely to contribute significantly to intrinsic rotation. This is because there are other symmetry-breaking mechanisms—namely, neoclassical flows [20–24] and finite

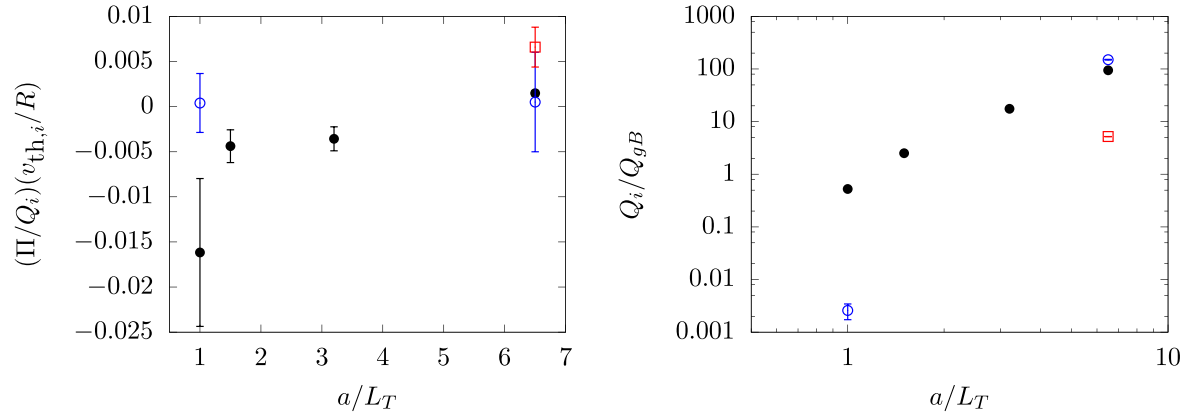

Figure 2. (Left): Ratio of ion momentum flux Π to ion heat flux Q_i as a function of a/L_T. (Right): Normalized ion heat flux as a function of a/L_T, with $Q_{\mathrm{gB}} \doteq n_i T_i v_{\mathrm{th},i}(\rho_i/a)^2$. Blue open circles indicate cases where the radial component of the magnetic drift was artificially set to zero, and the red square is a case where both the radial and bi-normal components of the magnetic drift were artificially set to zero. Error bars indicate statistical errors arising due to the finite interval used for the time average.

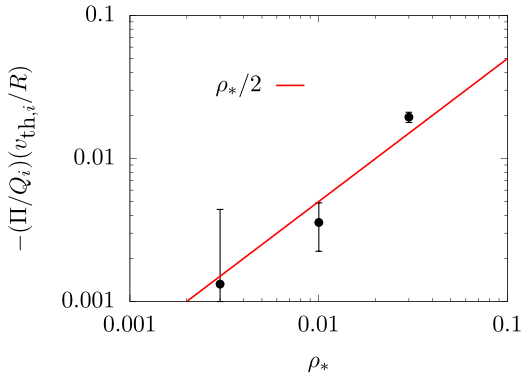

Figure 3. Ratio of ion momentum flux Π to ion heat flux Q_i as a function of $\rho_* = \rho_i/a$. Error bars indicate statistical errors arising due to the finite interval used for the time average.

orbit width effects [15–17]—that have been found analytically and numerically to drive Π/Q_i that scales as $(B/B_p)\rho_*$. As $B_p \ll B$ in most tokamaks, the associated momentum flux is likely an order of magnitude larger than the values obtained here. There are, however, a couple of caveats to consider. The scaling theory from section 4 was derived (and verified) under the assumption that turbulence is far from marginal. As such, it is not clear from theoretical considerations alone if one should expect additional factors of (B/B_p) appearing in the ρ_* scaling of the momentum flux near marginal stability. Of course, this study also only considered a single point in the parameter space; a broader range of parameters needs to be considered before a definitive statement about the importance of turbulent acceleration in generating intrinsic rotation can be made.

Finally, it is perhaps worth noting that the arguments used here to obtain the momentum flux scaling (14) lead to an identical result for the momentum flux driven by the slow poloidal variation of turbulence and by radial profile variation [15], both so-called 'global' effects. The discussion from section 5 also applies to these global effects, so that they too do not lead to momentum transport for a reduced system with no magnetic shear or radial magnetic drifts. As such, the results reported here for turbulent acceleration may provide some insight as to the size and scaling of the momentum flux driven by global effects.

Acknowledgments

The authors acknowledge the use of ARCHER through the Plasma HEC Consortium EPSRC grant number EP/L000237/1 under project e281-gs2 and the use of the EUROfusion High Performance Computer (Marconi-Fusion) under project MULTEI. This work was supported in part by the Engineering and Physical Sciences Research Council (EPSRC, Grant Number EP/R034737/1).

ORCID iDs

M Barnes https://orcid.org/0000-0002-0177-1689

References

[1] Rice J E, Bonoli P T, Goetz J A, Greenwald M J, Hutchinson I H, Marmar E S, Porkolab M, Wolfe S M, Wukitch S J and Chang C S 1999 Central impurity toroidal rotation in ICRF heated Alcator C-Mod plasmas *Nucl. Fusion* **39** 1175

[2] Rice J E, Hubbard A E, Hughes J W, Greenwald M J, LaBombard B, Irby J H, Lin Y, Marmar E S, Mossessian D and Wolfe S M 2005 The dependence of core rotation on magnetic configuration and the relation to the H-mode power threshold in Alcator C-Mod plasmas with no momentum input *Nucl. Fusion* **45** 251

[3] Bortolon A, Duval B P, Pochelon A and Scarabosio A 2006 Observation of spontaneous toroidal rotation inversion in ohmically heated tokamak plasmas *Phys. Rev. Lett.* **97** 235003

[4] Scarabosio A, Bortolon A, Duval B P, Karpushov A and Pochelon A 2006 Toroidal plasma rotation in the TCV tokamak *Plasma Phys. Control. Fusion* **48** 663

[5] deGrassie J S, Burrell K H, Groebner R J and Solomon W M 2007 Intrinsic rotation in DIII-D *Phys. Plasmas* **14** 056115

[6] Duval B P, Bortolon A, Karpushov A, Pitts R A, Pochelon A, Scarabosio A and the TCV Team 2007 Bulk plasma rotation in the TCV tokamak in the absence of external momentum input *Plasma Phys. Control. Fusion* **49** B195–209
[7] Rice J E *et al* 2007 Inter-machine comparison of intrinsic toroidal rotation in tokamaks *Nucl. Fusion* **47** 1618–24
[8] Eriksson L-G, Hellsten T, Nave M F F, Brzozowski J, Holmström K, Johnson T, Ongena J, Zastrow K-D and JET-EFDA Contributors 2009 Toroidal rotation in RF heated JET plasmas *Plasma Phys. Control. Fusion* **51** 044008
[9] Ince-Cushman A *et al* 2009 Observation of self-generated flows in tokamak plasmas with lower-hybrid-driven current *Phys. Rev. Lett.* **102** 035002
[10] Solomon W M *et al* 2010 Mechanisms for generating toroidal rotation in tokamaks without external momentum input *Phys. Plasmas* **17** 056108
[11] Parra F I, Nave M F F, Schekochihin A A, Giroud C, de Grassie J S, Severo J H F, de Vries P and Zastrow K-D 2012 Scaling of spontaneous rotation with temperature and plasma current in tokamaks *Phys. Rev. Lett.* **108** 095001
[12] Peeters A G and Angioni C 2005 Linear gyrokinetic calculations of toroidal momentum transport in a tokamak due to the ion temperature gradient mode *Phys. Plasmas* **12** 072515
[13] Parra F I, Barnes M and Peeters A G 2011 Up–down symmetry of the turbulent transport of toroidal angular momentum in tokamaks *Phys. Plasmas* **18** 062501
[14] Sugama H, Watanabe T H, Nunami M and Nishimura S 2011 Momentum balance and radial electric fields in axisymmetric and nonaxisymmetric toroidal plasmas *Plasma Phys. Control. Fusion* **53** 024004
[15] Parra F I and Barnes M 2015 Intrinsic rotation in tokamaks: theory *Plasma Phys. Control. Fusion* **57** 045002
[16] Parra F I, Catto P J and Barnes M 2011 Sources of intrinsic rotation in the low flow ordering *Nucl. Fusion* **51** 113001
[17] Parra F I, Barnes M, Calvo I and Catto P J 2012 Intrinsic rotation with gyrokinetic models *Phys. Plasmas* **19** 056116
[18] Calvo I and Parra F I 2012 Long-wavelength limit of gyrokinetics in a turbulent tokamak and its intrinsic ambipolarity *Plasma Phys. Control. Fusion* **54** 115007
[19] Calvo I and Parra F I 2015 Radial transport of toroidal angular momentum in tokamaks *Plasma Phys. Control. Fusion* **57** 075006
[20] Barnes M, Parra F I, Lee J P, Belli E A, Nave M F F and White A E 2013 Intrinsic rotation driven by non-Maxwellian equilibria in tokamak plasmas *Phys. Rev. Lett.* **111** 055005
[21] Lee J P, Barnes M, Parra F I, Belli E A and Candy J 2014 The effect of diamagnetic flows on turbulent driven ion toroidal rotation *Phys. Plasmas* **21** 056106
[22] Lee J P, Parra F I and Barnes M 2014 Turbulent momentum pinch of diamagnetic flows in a tokamak *Nucl. Fusion* **54** 022002
[23] Lee J P, Barnes M, Parra F I, Belli E A and Candy J 2015 Turbulent momentum transport due to neoclassical flows *Plasma Phys. Control. Fusion* **57** 125006
[24] Hornsby W A, Angioni C, Fable E, Manas P, McDermott R, Peeters A G, Barnes M, Parra F I and The ASDEX Upgrade Team 2017 On the effect of neoclassical flows on intrinsic momentum in asdex upgrade ohmic l-mode plasmas *Nucl. Fusion* **57** 046008
[25] Camenen Y *et al* 2011 Experimental evidence of momentum transport induced by up–down asymmetric magnetic equilibrium in toroidal plasmas *Nucl. Fusion* **51** 073039
[26] Ball J, Parra F I, Barnes M, Dorland W, Hammett G W, Rodrigues P and Loureiro N F 2014 Intrinsic momentum transport in up–down asymmetric tokamaks *Plasma Phys. Control. Fusion* **56** 095014
[27] Ball J, Parra F I and Barnes M 2016 Poloidal tilting symmetry of high order tokamak flux surface shaping in gyrokinetics *Plasma Phys. Control. Fusion* **58** 045023
[28] Ball J and Parra F I 2016 Scaling of up–down asymmetric turbulent momentum flux with poloidal shaping mode number in tokamaks *Plasma Phys. Control. Fusion* **58** 055016
[29] Ball J, Parra F I, Lee J P and Cerfon A J 2016 Effect of the Sharfanov shift and the gradient of β on intrinsic momentum transport in up–down asymmetric tokamaks *Plasma Phys. Control. Fusion* **58** 125015
[30] Ball J and Parra F I 2017 Turbulent momentum transport due to the beating between different tokamak flux surface shaping effects *Plasma Phys. Control. Fusion* **59** 024007
[31] Ball J, Parra F I, Landreman M and Barnes M 2017 Optimized up–down asymmetry to drive fast intrinsic rotation in tokamaks *Nucl. Fusion* **58** 026003
[32] Sung T, Buchholz R, Casson F J, Fable E, Grosshauser S R, Hornsby W, Migliano P and Peeters A G 2013 Toroidal momentum transport in a tokamak caused by symmetry breaking parallel derivatives *Phys. Plasmas* **20** 042506
[33] Waltz R E, Staebler G M and Solomon W M 2011 Gyrokinetic simulation of momentum transport with residual stress from diamagnetic level velocity shears *Phys. Plasmas* **18** 042504
[34] Camenen Y, Idomura Y, Jolliet S and Peeters A G 2011 Consequences of profile shearing on toroidal momentum transport *Nucl. Fusion* **51** 073039
[35] Grierson B A, Wang W X, Ethier S, Staebler G M, Battaglia D J, Boedo J A, deGrassieand J S and Solomon W M 2017 Main-ion intrinsic toroidal rotation profile driven by residual stress torque from ion temperature gradient turbulence in the DIII-D tokamak *Phys. Rev. Lett.* **118** 015002
[36] Hornsby W A, Angioni C, Lu Z X, Fable E, Erofeev I, McDermott R, Medvedeva A, Lebschy A and The ASDEX Upgrade Team 2018 Global gyrokinetic simulations of intrinsic rotation in ASDEX Upgrade Ohmic L-mode plasmas *Nucl. Fusion* **58** 056008
[37] Kniep J C, Leboeuf J-N and Decyk V K 2004 Gyrokinetic particle-in-cell calculations of ion temperature gradient driven turbulence with parallel nonlinearity and strong flow corrections *Comput. Phys. Commun.* **164** 98
[38] Lin Z, Rewoldt G, Ethier S, Hahm T S, Lee W W, Lewandowski J, Nishimura Y and Wang W X 2005 Particle-in-cell simulations of electron transport from plasma turbulence: recent progress in gyrokinetic particle simulations of turbulent plasmas *J. Phys.: Conf. Ser.* **16** 16
[39] Candy J, Waltz R, Parker S E and Chen Y 2006 Relevance of the parallel nonlinearity in gyrokinetic simulations of tokamak plasmas *Phys. Plasmas* **13** 074501
[40] Barnes M, Parra F I and Landreman M 2018 Stella: a mixed implicit-explicit δf-gyrokinetic code for general magnetic field configurations *J. Comput. Phys.* submitted (arxiv:1806.02162)
[41] Catto P J 1978 Linearized gyro-kinetics *Plasma Phys.* **20** 719
[42] Frieman E A and Chen L 1982 Nonlinear gyrokinetic equations for low-frequency electromagnetic waves in general plasma equilibria *Phys. Fluids* **25** 502
[43] Brizard A J and Hahm T S 2007 Foundations of nonlinear gyrokinetic theory *Rev. Mod. Phys.* **79** 421
[44] Parra F I and Catto P J 2008 Limitations of gyrokinetics on transport time scales *Plasma Phys. Control. Fusion* **50** 065014
[45] Parra F I and Calvo I 2011 Phase-space lagrangian derivation of electrostatic gyrokinetics in general geometry *Plasma Phys. Control. Fusion* **53** 045001
[46] Abel I G, Plunk G G, Wang E, Barnes M, Cowley S C, Dorland W and Schekochihin A A 2013 Multiscale

gyrokinetics for rotating tokamak plasmas: fluctuations, transport, and energy flows *Rep. Prog. Phys.* **76** 116201
[47] Barnes M, Parra F I and Schekochihin A A 2011 Critically balanced ion temperature gradient turbulence in fusion plasmas *Phys. Rev. Lett.* **107** 115003
[48] Goldreich P and Sridhar S 1995 Toward a theory of interstellar turbulence: II. Strong alfvenic turbulence *Astrophys. J.* **438** 763–75
[49] Mandell N R, Dorland W and Landreman M 2018 Laguerre–Hermite pseudo-spectral velocity formulation of gyrokinetics *J. Plasma Phys.* **84** 905840108
[50] Dougherty J P 1964 Model Fokker–Planck equation for a plasma and its solution *Phys. Fluids* **7** 1788
[51] Miller R L, Chu M S, Greene J M, Lin-Liu Y R and Waltz R E 1998 Noncircular, finite aspect ratio, local equilibrium model *Phys. Plasmas* **5** 973